

RSC Advances



This is an *Accepted Manuscript*, which has been through the Royal Society of Chemistry peer review process and has been accepted for publication.

Accepted Manuscripts are published online shortly after acceptance, before technical editing, formatting and proof reading. Using this free service, authors can make their results available to the community, in citable form, before we publish the edited article. This *Accepted Manuscript* will be replaced by the edited, formatted and paginated article as soon as this is available.

You can find more information about *Accepted Manuscripts* in the [Information for Authors](#).

Please note that technical editing may introduce minor changes to the text and/or graphics, which may alter content. The journal's standard [Terms & Conditions](#) and the [Ethical guidelines](#) still apply. In no event shall the Royal Society of Chemistry be held responsible for any errors or omissions in this *Accepted Manuscript* or any consequences arising from the use of any information it contains.



Fabrication of high density graphene aerogel-gold nanostars hybrid and its application for the electrochemical detection of hydroquinone and o-dihydroxybenzene

Bei Hongxia,^a Li Ruiyi,^a Li Zaijun,^{*a,b} Liu Junkang,^a Gu Zhiguo^a and Wang Guangli^a

Received 00th January 20xx,
Accepted 00th January 20xx

DOI: 10.1039/x0xx00000x

www.rsc.org/

Graphene aerogel materials have attracted increasing attention owing to their large specific surface area, high conductivity and electronic interactions. In the study, we for the first time reported a new strategy for the fabrication of high density graphene aerogel (HDGA) through a simple multiple gel method. The result shows that the density of HDGA will rapidly increase with increasing time of the graphene oxide gelation cycle. The as-prepared HDGA exhibits a better mechanical strength and electrochemical property when common graphene aerogel. Interestingly, these properties are easy to be adjusted by controlling time of the graphene oxide gelation cycle. To further improve the electrocatalytic performance, gold nanostars were synthesized and modified on the surface of graphene sheets. The hybrid was successfully developed as a sensing material for the electrochemical detection of hydroquinone and o-dihydroxybenzene with ultrahigh sensitivity and selectivity. The study also opens an avenue for the design and synthesis of various graphene aerogel materials to meet the needs of further applications in sensing, catalysis and energy storage/conversion device.

1 Introduction

With the development of nanoscience and nanotechnology, many efforts have been made to design and prepare novel composite nanomaterials with the desired properties playing essential roles in science and technology. To obtain such nanocomposites, it is necessary to hybridize materials with different properties and novel hybrid nanomaterials new functional and high-performance could be obtained due to the synergistic effect between or among the different properties.¹ At present, graphene-based hybrids have become a hot research topic in material science, because the hybridization can be an effective strategy to enhance the functionality of materials and the integration of nanomaterials on graphene nanosheets potentially paves a new way to improve their electronic, chemical and electrochemical properties.² Graphene is a versatile two-dimensional carbon nanomaterial formed by sp² bonded carbon atoms which were arranged in a single-layer hexagonal lattice. And it has drawn exponentially growing interests and hold great promise for many potentially important applications.³ To date, many graphene-based hybrids, including graphene-gold clusters for oxygen reduction reaction,⁴ graphene-gold nanoparticles for sensing,⁵ graphene-cobalt porphyrin for oxygen reduction reaction,⁶ graphene-metal oxide nanoparticles for capacitive deionization of saline water,⁷ and N-doped graphene-PtRu nanoparticles as high performance anode for direct methanol fuel cells,⁸ were synthesized. Although there are great number of reports relating to graphene-based hybrid synthesis in literatures, but the fabrication of graphene-based hybrids with special property and structure is still highly attention.

Owing to large specific surface area, high conductivity, electronic interactions and mechanical strength, graphene aerogel (GA)-based hybrids recently received a great attention⁹ and demonstrated greatly potential applications in many fields such as sensing,¹⁰ supercapacitor,¹¹ thermal energy storage,¹² electrocatalyst,¹³ lithium-ion battery,¹⁴ adsorbent,¹⁵ air purification,¹⁶ thermal management¹⁷ and fuel cell.¹⁸ However, the current three-dimensional graphene products suffer from poor electronic conductivity, low surface area and insufficient mechanical strength. To meet the need of further applications that require high electronic conductivity and high mechanical strength, many efforts have been attempted to fabricate various GA-based hybrids. The first method is to use small molecular chemical reagents containing special groups as the crosslinking agent to connect graphene sheets into whole structure. For example, Li and co-workers developed a compressive graphene aerogels that were obtained by the one-step reduction and self-assembly of graphene oxide with ethylenediamine and then freeze-drying.¹⁹ The GA holds good compressibility, variable electrical resistance and fire-resistance. The high porosity with a hydrophobic nature allows the GA absorb different organic liquids, and the absorption-squeezing process has been demonstrated for the oil collection. The second method is to introduce polymer into GA for enhancing the mechanical strength. For example, Xiao and co-workers reported a scalable and modular method to prepare a new type of sandwich-structured graphene-based nanohybrid paper and explore its practical application as high-performance electrode in the flexible supercapacitor.²⁰ The freestanding and flexible graphene paper was firstly fabricated by highly reproducible

printing technique and bubbling delamination method, by which the area and thickness of graphene paper can be freely adjusted in a wide range. The as-prepared graphene paper possesses a collection of unique properties of highly electronic conductivity, light weight and excellent mechanical properties. Moreover, Fang and co-workers reported a three-dimensional graphene-based macro- and mesoporous frameworks for high performance electrochemical capacitive energy storage.²¹ The mesopores are generated by silica networks uniformly grown on the surface of graphene. The resulting GA exhibits a narrow mesopore size distribution, high surface area, and low mass density. The third method is to introduce conducting polymer into GA for improving the electronic conductivity. For example, Ye and Feng reported a self-assembled three-dimensional hierarchical graphene/polypyrrole nanotube hybrid aerogel and its application for supercapacitors.²² The investigation shows that the addition of polypyrrole obviously improves the electronic conductivity. However, the electronic conductivity and mechanical strength of GA materials cannot be improved significantly via only relying on above methods. In fact, present technologies can only get ultralight GA. The ultralight characteristic will inevitably lead to poor mechanical strength and electronic conductivity owing to its sparse graphene sheets and fragile frame structure. As is well-known, graphene sheet itself has excellent electrical and mechanical properties, increase the density is one of the most simple and effective method for largely enhancing the mechanical strength and electronic conductivity. Limited to low water-solubility of graphite oxide, no an ideal way can substantially achieve to prepare high density GA up to now.

Herein, we reported a new strategy for the fabrication of high density graphene aerogel (HDGA). The as-prepared HDGA exhibits a better mechanical strength and electrochemical property compared with common graphene aerogel. The HDGA-gold nanostars hybrid was successfully applied for the electrochemical detection of hydroquinone and o-dihydroxybenzene.

2 Experimental

2.1 Materials and reagents

Chlorauric acid, citric acid, ascorbic acid, hydroquinone (HQ), o-dihydroxybenzene (DHB) and resorcinol (RC) were purchased from Sigma-Aldrich Chemical Company (Mainland, China). Graphite oxide (GO) was prepared from natural graphite by a modified Hummers' method.²³ Phosphate-buffered saline (PBS, pH 7.0, Na₂HPO₄-KH₂PO₄-NaCl-KCl, 0.01 M) was prepared in the laboratory. The chitosan solution was prepared by dissolving 5.0 g of chitosan in 100 ml of 1.0% (v/v) acetic acid. All other reagents employed were of analytical reagent grade or with the highest quality and were purchased from Shanghai Chemical Company (Shanghai, China). Ultra pure water (18.2 MΩ cm) purified from a Milli-Q purification system was used throughout the experiment.

2.2 Material characterization

Scanning electron microscope (SEM) analysis was carried out in HITACHI S4800 field emission scanning electron microscope. SEM sample was prepared by placing a drop of dilute ethanol dispersion of the composites onto a copper plate attached to an aluminum sample holder, and the solvent was allowed to evaporate at room temperature. Transmission electron microscope (TEM) images were conducted on a JEOL 2010 transmission electron microscope at 200 keV. The sample was prepared by dispensing a small amount of dry powder in ethanol. Then, one drop of the suspension was dropped on 300 mesh copper. TEM grids covered with thin amorphous carbon films. X-ray diffraction (XRD) patterns were measured on a X-ray D8 Advance Instrument operated at 40 kV and 20 mA and using Cu K α radiation source with $\lambda=0.15406$ nm. Raman measurements were carried out using a InVia laser micro-Raman spectrometer. X-ray photoelectron spectroscopy (XPS) measurements were performed by using a PHI 5700 ESCA spectrometer with monochromated Al KR radiation ($h\nu=1486.6$ eV). The N₂ adsorption and desorption isotherms were measured at 77 K on a Quantachrome Nova 2000. Prior to the gas sorption measurements, all the samples were outgassed in vacuum at 120°C for 24 h. The specific surface area and the pore size distribution were calculated using the Braunauer-Emmett-Teller (BET) method and the relative pressure range of p/p_0 from 0.1 to 0.3 was used for multipoint BET calculations. Non-local density functional theory assuming the pores are slit/cylinder shaped was used to determine the pore size distribution and mesopore volume.

2.3 The preparation of HDGA

The synthesis of HDGA includes four assembly processes. First process is to disperse the mixture of 0.2 g GO with 0.6 g ascorbic acid in 50 ml of ultrapure water under ultrasonic condition to form homogeneous GO dispersion. Followed heating at 40°C for 16 h to produce graphene hydrogel. The hydrogel was treated by freeze-drying to produce GA-1.²¹ Second process is to prick holes in the face of GA-1 by fine steel needles ($\phi=1$ mm). Next, GA-1 was placed into another glass vial with a plug, which its inner volume consistent with the volume of GA-1. The third process is to add 30 ml of the mixed solution of GO (0.12 g) and ascorbic acid (0.36 g) into the GA-1. Followed by heating at 40°C for 16 h and freeze drying to obtain GA-2. Fourth process is to repeat above second process and third process until time of the GO gelation cycle reach to a desired value. Finally, it was reduced by thermal annealing at 600°C in Ar/H₂ (95:5) for 4 h to obtain HDGA. Based on time (n) of the cycle during the synthesis, the product is designated as HDGA-n.

2.4 The synthesis of HDGA-gold nanostars nanohybrid

Gold nanostars (GNSs) were prepared by the seed growth method. In a typical synthesis, 10 ml of chloroauric acid solution (4 mg/ml) was mixed with 5 ml of citrate acid solution (30 mg/ml) and 5 ml of tannic acid solution (1.0 mg/ml). The mixed solution was heated at 70°C. When the solution turned into clear crimson, the temperature was rapidly raised to 100°C. To obtain a gold seed solution, the temperature was

kept for 5 min and then cooled in air to room temperature. In another glass vial, 25 μ l of citrate acid solution (0.05 M) was incubated with 50 μ l of chloroauric acid solution (0.03 M) in 2.5 ml of ultrapure water for 5 minutes under stirring at 1000 rpm. After added 30 μ l of silver nitrate (0.01 M), 2.5 ml of hydrogen peroxide (30%) was rapidly added. Followed by injecting 10 μ l of the gold seed solution. After about 30-40s, the stirring was stopped to obtain a GNS solution. Its absorption spectrum was measured and shown in Fig.s1.

The dried HDGA-n was immersed in the GNS solution. After all of the GNS solution was sucked into HDGA-n, it dry by freeze-drying at -50 $^{\circ}$ C for 12 h to obtain HDGA-n/GNS.

2.5 The density measurement

Densities (ρ) of the HDGA-n could be determined from the mass weight divided by the volume. Here, the averaged values of data were used. The volumes (v) of cylindrical shaped aerogel HDGA-n was calculated based on the equation (1):

$$v = \pi \left(\frac{d}{2}\right)^2 h \quad (1)$$

where, d refers to the diameter of the HDGA-n, and h represents the height of the HDGA-n. The densities ρ of the HDGA-n were calculated from equation (2):

$$\rho = \frac{m}{v} \quad (2)$$

m refers to the mass of the HDGA-n obtained by the precision balance.

2.6 Electrochemical measurements

Electrochemical experiments were performed with a CHI660D electrochemical workstation (Shanghai, China). Conventional three electrode system was used for cyclic voltammetry (CV) with Ag/AgCl (saturated KCl) electrode as the reference electrode, platinum wire as the counter electrode, and bare or modified glassy carbon electrode (GCE, 1.0 mm in diameter) as the working electrode. Before use, GCE was polished successively with 1.0, 0.3, and 0.05 μ m alumina powder, and sonicated in a 6.0 M of nitric acid/doubly distilled water and ethanol/doubly distilled water for 20 min. Then, the GCE as working electrode was subjected to cyclic scanning in 0.5 M of sulphuric acid solution in a potential range from -0.1 V to 1.0 V. When the cyclic voltammogram was almost unchanged, the electrode was taken out, cleaned with ultra pure water and dried in a stream of nitrogen. The treated GCE was modified with different graphene material to prepare different sensor using the following procedure: the HDGA-n/GNS sample was dissolved in ethyl acetate to make up 0.2 mg ml⁻¹ solution, then 10 μ l of the mixed solution was dropped on the surface of GCE. After that, 2 μ l of chitosan solution was carefully spreading on the HDGA-n/GNS surface of GCE and dried in air before use. The electrochemical experiment was carried out under room temperature, and all experimental solution was degassed by nitrogen for at least 15 min. Then, a nitrogen atmosphere was maintained during electrochemical measurements.

3 Results and discussion

3.1 Hybrid synthesis

HDGA was fabricated through the use of a simple multiple gel method. The synthesis includes four assembly processes (shown in Fig.1). The first process is to disperse the mixture of GO with ascorbic acid in ultrapure water under the ultrasonic condition to form a homogeneous GO dispersion. Followed heating to produce the graphene hydrogel. The hydrogel was treated by freeze-drying to produce GA-1. Second process is to

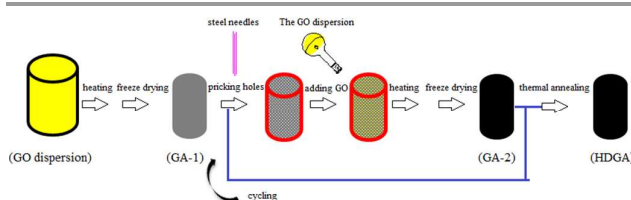


Fig.1 The procedure for synthesis of HDGA.

prick hole in the face of GA-1 by fine steel needles. The formed small holes play important roles in the fabrication of HDGA. As a rule, GA has a dense and smooth surface with few open holes and high hydrophobic property. The characteristic makes GO dispersion is difficult to enter into the interior of GA for the next GO gelation. However, prick hole can effectively resolve the problem. The pricking hole breaks the most of closed pores in the GA internal to produce a great number of open holes. These open holes make the GO dispersion can reach all parts of GA. This will largely increase the volume of GO dispersion that can enter into old GA during the following synthesis. For the multiple gel method, the introduction of a bigger volume of the GO dispersion brings more increase on the density. Because there is a highly developed network of open pore structures in the interior of GA, the GO dispersion is very easy to enter into the interior of GA if the closed pores on the face of GA were broken by the needles. The investigation demonstrates that further increase of number of the pricked holes can not obviously improve the synthesis when the number of the pricked holes is more than 5 per square centimetre. Next, GA-1 was placed into another glass vial with a plug. The investigation reveals that the volume of glass vial is a key factor to influence on the increase on the density. The use of a relatively big vial results in a very small change on the density of product for the synthesis. The resulting product displays a concentric circle structure in the absence of pricked holes, verifying that new GA was formed in the periphery of old GA but not in the internal, or swollen shape in the absence of pricked pores, owing to the outward tension caused by volume expansion (shown in Fig.s2). However, the problem can be resolved by the use of relatively small vial as a mold for the synthesis. Such a mold makes newly formed GA can only grow in internal of old GA, thus resulting in an obvious increase on the density. To reduce the space between GA-1 and wall of the via, the inner volume of vial is well matched with the size of GA-1 in the study. The third process is to add 30 ml of the mixed solution of GO and ascorbic acid into the GA-1. Followed by heating and freeze drying to obtain GA-2.

Fourth process is to repeat above second process and third process until time of the GO gelation cycle reach to the desired value. Finally, it was reduced by thermal annealing in Ar/H₂ to obtain HDGA. Based on time (n) of the GO gelation cycle during the synthesis, the product is designated as HDGA-n. Mechanical strength and electrical properties of the as-prepared GA samples were investigated. Fig.2A shows the density of different sample synthesized through the use of different time of the GO gelation cycle. It can be seen that the density rapidly increases with increasing time of the cycle. The each cycle brings an almost equal increment on the density. This is because an equal volume (30 ml) of the GO dispersion can be added into old GA for the each of the GO gelation when time of the cycle is less than ten, the each cycle will produce an equal of mass change (about 0.12 g). During the cycle process, new graphene framework was formed in situ in old graphene framework. Thus, new framework and old framework intertwined each other to form a whole network structure. This will greatly enhance the mechanical properties, which was well confirmed by the result of maximum bearing weight test (see Fig.2B). At the same time, the big pores in HDGA were also changed into relatively small pores. With increasing time of the cycle, HDGA will display smaller and denser pore structure with narrow pore size distribution.

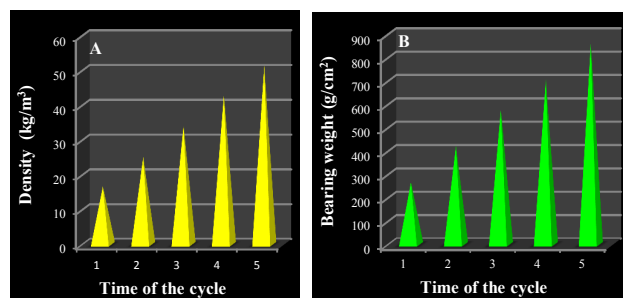


Fig.2 Density (A) and maximum bearing weight (B) of different HDGA sample prepared by the use of different time of the cycle.

Fig.3A indicates the resistance and differential pulse voltammetry (DPV) curve of different HDGA prepared by different time of the cycle. From Fig.3A, we observe that the resistance rapidly reduces with increasing time of the cycle. This is because the graphene sheet junctions facilitates much faster charge transport with increasing time of the cycle, which improves the electronic conductivity and results in decrease of the resistance. To further examine on the effect of time of the cycle on the electrical property, several kinds of HDGA materials were used as sensing material for catalyzing the oxidation/reduction of $\text{Fe}(\text{CN})_6^{4-}/\text{Fe}(\text{CN})_6^{3-}$, respectively. Fig.3B presents DPV curves of the electrode modified with different HDGA material. The result shows that DPV response of the electrode increases with the increase of the cycle time, indicating that the HDGA prepared by using more time of the cycle can offer a better electrocatalytic ability. Moreover, the result also reveals that the catalytic activity of HDGA is greatly higher than that of both graphene and GA (see Fig.4). The above results have demonstrated that HDGA is of excellent

mechanical and electrical properties. More importantly, its property can be conveniently adjusted by controlling time of the cycles.

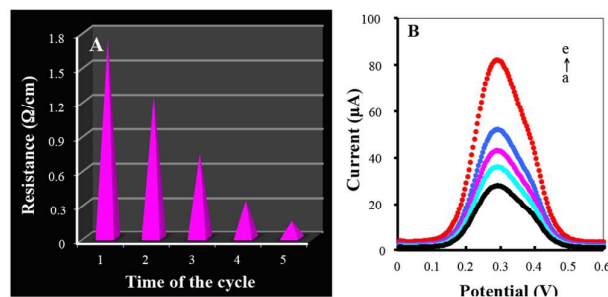


Fig.3 The resistance (A) and DPV curve (B) of different HDGA material obtained by the use of different time of the GO gelation cycle. Time of the cycle: 1, 2, 3, 4 and 5 (from a to e). The DPV parameters were set to a scan rate of 4 mV/s, 50 mV pulse amplitude, 20 ms pulse width and -0.2 V initial potential. The pH 7.0 PBS containing 1.0 mM of $[\text{Fe}(\text{CN})_6]^{3-/4-}$.

The obtained HDGA-n was immersed in the GNS solution. After all of the GNS solution was sucked into HDGA-n, it dry by freeze-drying to obtain HDGA-n/GNS hybrid.

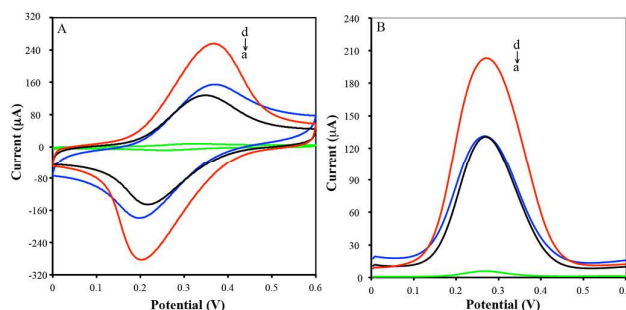


Fig.4 CVs (A) and DPV curves (B) of bare GCE electrode (a) and the modified electrode with graphene (b), GA (c) and HDGA (d) in pH 7.0 PBS containing 1.0 mM of $[\text{Fe}(\text{CN})_6]^{3-/4-}$. The DPV parameters were set to a scan rate of 4 mV/s, 50 mV pulse amplitude, 20 ms pulse width and -0.2 V initial potential.

3.2 Structure characterization

Fig.5 presents typically SEM and TEM images of the as-prepared HDGA-5/GNS. The SEM analysis shows that the HDGA-5 gives a rather thin, well-defined, and interconnected three-dimensional network microstructure with dispersed pores of several micrometers in the diameter, suggesting efficient assembly of GO sheets during the hydrothermal reaction. GNSs are well dispersed on the wrinkled graphene sheets. The GNS offers a unique structure with rod-like spikes randomly protruding outwards. TEM analysis further demonstrates that the GNSs has an average particle size of about 100 nm and its surface exists a rich of sharp edges and tips. The gold nanocrystals with sharp edges and tips can offer stronger localized surface plasmon resonance compared with gold nanoparticles with a smooth and flat surface. Thus, the characteristic of GNS will lead to an enhanced electrocatalytic activity.

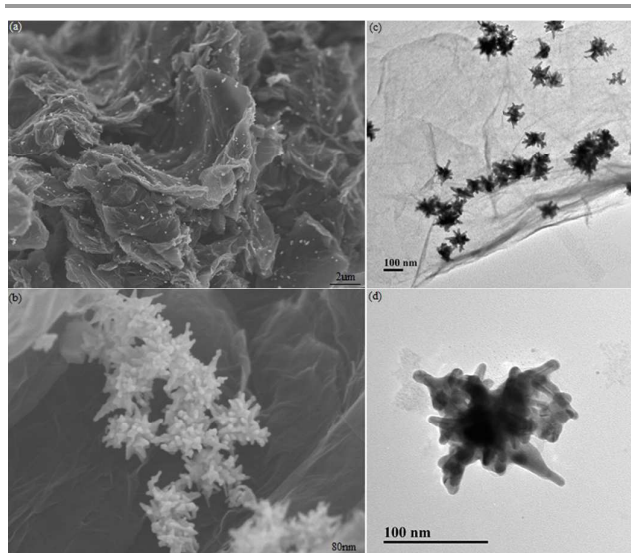


Fig.5 The SEM (a and b) and TEM images (c and d) of HDGA-5/GNS hybrid

The XRD pattern of HDGA-5/GNS was shown in Fig.6. There are four sharp diffraction peaks on the XRD pattern at scattering angles of 38.28° , 44.48° , 64.6° and 77.64° , corresponding to crystal planes Au (111), Au (200), Au (220) and Au (311) of gold face-centered cubic crystallographic structure (JCPDS card No. 65-2870). Moreover, we also noted that these GNSs were anchored on surface of the wall in the HDGA-5 rather than enwrapped by graphene sheets. This could provide more abundant active sites for the electrocatalytic reduction events and result in an increase of the sensitivity. There are two typical Raman peaks of graphene materials on the Raman spectrum, including D band (1320 cm^{-1}) and G band (1591 cm^{-1}). Moreover, high I_D/I_G intensity ratio (1.57) for HDGA-5 was also obtained, indicating a decrease in size of the in-plane sp^2 domains and the removal of the oxygen functional groups in the reduced graphene oxide during the thermal annealing.

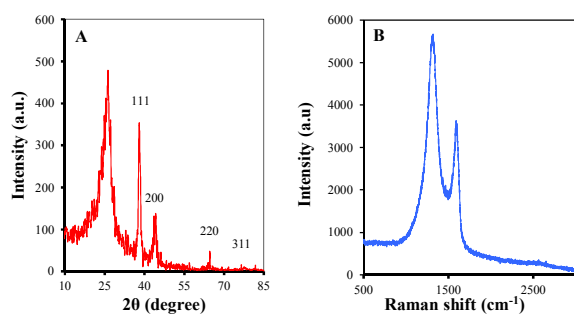


Fig.6 XRD pattern (A) and Raman spectrum (B) of HDGA-5/GNS

State-of-the-art surface and pore-size characterization of the HDGA-5/GNS were performed by nitrogen adsorption/desorption experiments with advanced methods based on the density functional theory. The type IV nitrogen adsorption/desorption isotherm of HDGA-5/GNS shows a hysteresis loop at high relative pressure (shown in Fig.7A), indicating the existence of plentiful mesoporous structures in the aerogel.

According to the NLDFT method, the pore size distribution has a sharp peaks at 80 nm (shown in Fig.7B). The broad pore size distribution, spanning from several to 200 nm, implies that the aerogel is rich in hierarchical pores. The macropores could originate from the interconnected hollow space, and the mesopores could be generated by the wrinkled morphology of graphene sheets. The HDGA-5/GNS has experienced five times of graphene oxide gelation cycle, the aerogel become very dense. Thus, we don't find any micron order of the macropores in the HDGA-5/GNS. The BET surface area of HDGA-5/GNS was found to be $1022\text{ m}^2\text{ g}^{-1}$. The high surface area will largely accelerate the electron transfer and the mass transport during the electrochemical reaction.

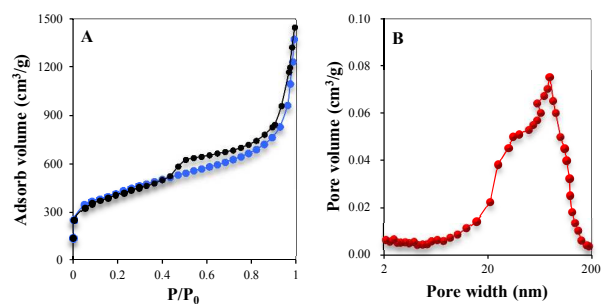


Fig.7 Nitrogen adsorption/desorption isotherm (A) and pore-size distribution curve for N_2 (B) of HDGA-5/GNS.

XPS technology is a powerful tool for studying on the surface chemical properties of materials. Fig.8 presents total, C_{1s} and Au_{4f} XPS spectra of the HDGA-5/GNS. The total XPS spectrum contains four peaks at 83.5, 87.3, 284.4 and 531.9 eV. The peaks at 284.4 and 531.9 eV could be assigned to C_{1s} and O_{1s} , which come from graphene. The peaks at 83.5 and 87.3 eV

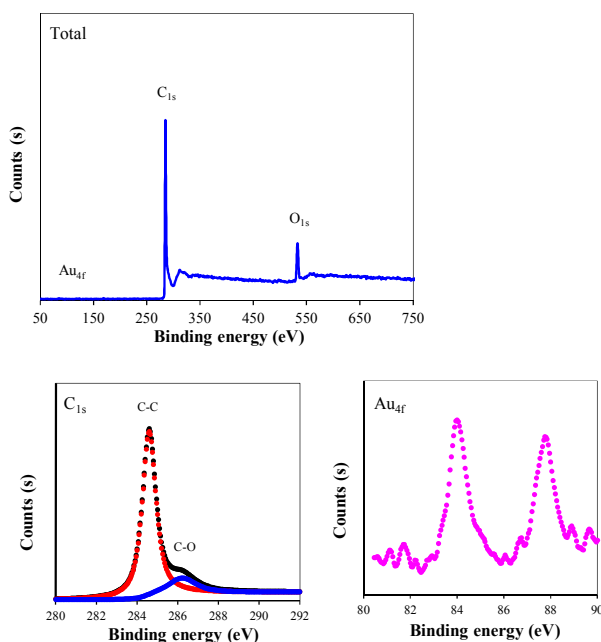


Fig.8 The total, C_{1s} and Au_{4f} XPS spectra of the HDGA-5/GNS

could be assigned to Au4f, which come from GNS in the hybrid. On the C_{1s} XPS spectrum, the peaks located at 284.6 and 286.6 eV can be assigned to C-C and C-O species.²⁴

3.3 Electrochemical property

HQ, DHB and RC were employed as the model compounds for evaluating the electro-catalytic performance of HDGA-5/GNS. Herein, the sensor based on the HDGA-5/GNS was fabricated and its electrochemical performances were investigated by cyclic voltammetry (CV) and differential pulse voltammetry (DPV) towards HQ, DHB and RC, respectively. Fig.9A presents typically CV curves of the sensor in pH 7.0 PBS containing in pH 7 PBS containing 0.0, RC, 1.2×10^{-5} HQ, DHB or the mixture of HQ and DHB. Fig.9A shows that three kinds of compounds exhibits different CV performance. No any obvious peak can be observed on the CV curve of RC. Although there are a pair of reversible redox peaks on the CV curves of both HQ and DHB, their peak potentials of the oxidation/reduction exist relatively big difference. The feature can be used to selectively determine HQ and DHB in the mixture of HQ, DHB and RC. Compared with bare glassy carbon electrode, the HDGA-5/GNS sensor gives remarkably enhanced peak currents for HQ and DHB, indicating that the HDGA-5/GNS offers high electrocatalytic activity towards oxidation/reduction of HQ and DH. Fig.9A indicates the current peaks in the CV curves of HQ and DHB exist some overlap, which may lead to mutual interference for electrochemical detection of HQ and DHB. To resolve the problem, DPV behaviour of the sensor was investigated in pH 7.0 PBS containing 1.2×10^{-5} M of HQ, 1.2×10^{-5} M of DHB and 1.2×10^{-5} M of RC. Fig.9B displays DPV curve of the RC is almost a straight line with any current peak, which demonstrates that the RC don't interfere with detection of HQ and DHB by the DPV method. However, DPV curves of HQ and DHB have sensitive current peaks. The separation of current peaks between HQ and DHB arrives at about 112 mV, which is large enough to separation the two components. Because DPV method offers a higher current response and better resolution than the CV method, it was applied to synchronously detect HQ and DHB.

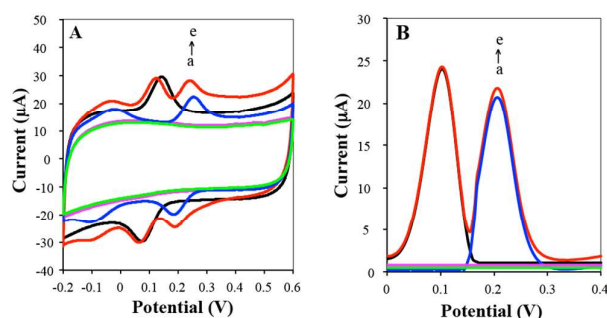


Fig.9 CV (A) and DPV (b) curves of the sensor based on the HDGA-5/GNS in pH 7 PBS containing 0.0, RC (b), 1.2×10^{-5} HQ (c), DHB (c) or the mixture of HQ and DHB (e). The DPV parameters were set to a scan rate of 4 mV/s, 50 mV pulse amplitude, 20 ms pulse width and -0.2 V initial potential.

Since proton takes part in the electrochemical reaction, acidity of the electrolyte is considered to significantly affect the

electrochemical behaviors of HQ and DHB.²⁵ In the study, the CVs of HQ and DHB at different pH solutions were tested in the range from 4.0 to 9.0. As shown in Fig.s3, the oxidation peak potentials of the two isomers shift to lower values with the increase in pH values and these peak potentials decreases linearly with the rising pH values. The regression equations and correlation coefficients for these lines are $E_p = 0.856 - 0.085 \text{ pH}$ ($R = 0.998$) for HQ, and $E_p = 0.983 - 0.084 \text{ pH}$ ($R = 0.999$) for DHB. The result further confirms that protons participate in the redox processes of HQ and DHB at the sensor. Because two lines are almost parallel, indicating that the difference of the potential was constant, the simultaneous detection of HQ and DHB is possible in a broad range at the sensor. However, a high oxidation potential at low pH may lead to serious interference for real sample analysis. In view of the stability of HQ and DHB, a weak acidic solution was better for this experiment. Therefore, the PBS solution of pH 7.0 was used as a supporting electrolyte for the electrochemical measurements.

3.4 Analytical characteristics

Fig.10A shows DPV curves of the sensor in the PBS containing different concentration of HQ and DHB. The peak current (I_p) is linear to the concentration of HQ in the range of 1×10^{-9} – 9×10^{-5} M. The corresponding linear regression equations is expressed in the following equation: $I_p = -0.8902C - 9.267$, with a statistically significant correlation coefficient of 0.9999, where I_p is the DPV peak current in μA and C is the concentration of HQ in the unit of μM ; The I_p is linear to the concentration of DHB in the range of 1.0×10^{-9} – 9×10^{-5} M. Corresponding linear regression equations is expressed in the following equation: $I_p = -1.165C - 10.817$, with a statistically significant correlation coefficient of 0.9998, where I_p is the DPV peak current in μA and C is the concentration of DHB in the unit of μM . The detection limit is 4.3×10^{-10} M for HQ and 2.1×10^{-10} M for DHB that were obtained from the signal-to-noise characteristics of these data ($S/N=3$). The above results proved that the HDGA-5 possessed preferable electro-activity in neutral media and displayed an excellent electro-catalytic activity towards the oxidation/reduction of HQ and DHB.

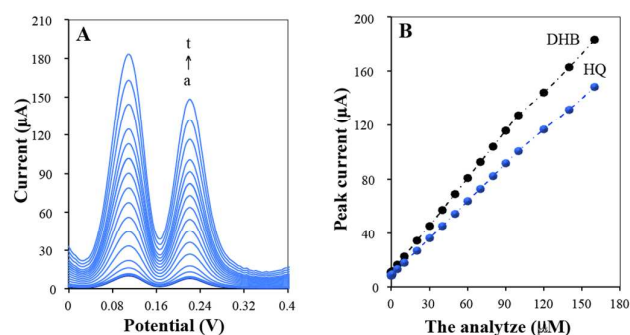


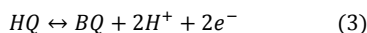
Fig.10 DPVs of the sensor in PBS containing 0.0, 1×10^{-9} , 5×10^{-9} , 1×10^{-8} , 5×10^{-8} , 1.0×10^{-7} , 5×10^{-7} , 1.0×10^{-6} , 5.0×10^{-6} , 1.0×10^{-5} , 2.0×10^{-5} , 3.0×10^{-5} , 4.0×10^{-5} , 5.0×10^{-5} , 6.0×10^{-5} , 7.0×10^{-5} , 8×10^{-5} , 9×10^{-5} , 1×10^{-4} , 1.2×10^{-4} , 1.4×10^{-4} and 1.6×10^{-4} DHB and HQ (from a to t)(A). B: calibration plots of concentration of DHB and HQ vs. peak current change (ΔI_p). The DPV parameters were set to a scan rate of 4 mV/s, 50 mV pulse amplitude, 20 ms pulse width and -0.2 v initial potential.

Relative standard deviation (RSD%) of the sensor in successive eleven scans for HQ and DHB are 0.89% and 1.22%, respectively. Twenty sensors were prepared independently under the same operating conditions, revealing an acceptable reproducibility with RSD 1.8% and 2.2% for HQ and DHB. Finally, the stability of modified electrode was examined by storing it in a place at 4 °C for four weeks. The peak current remained 98.7% of originally measured value. These results confirm excellent reproducibility and stability.

The interference from possible cations and anions existed in natural water were investigated. Ca^{2+} , Mg^{2+} , Na^+ , K^+ , SO_4^{2-} , CO_3^{2-} , NO_3^- , PO_4^{3-} , $\text{C}_2\text{O}_4^{2-}$ and Cl^- are main ions in natural water. Because of very low reduction potential, these ions cannot be reduced in the potential range of 0.0-0.30 V, 2000-fold the above ions brings a less than 1% change of DPV response for the detection of HQ and DHB. Fe^{3+} , Co^{2+} , Ni^{2+} and Cu^{2+} exist in natural water at trace level. These ions can combine with PO_4^{3-} ion in the PBS to form stable complex, thus resulting to further decrease of the reduction potential. The result shows that 100-fold the above ions cause a less than 3% change of the DPV signal for the detection of HQ and DHB. RC often coexists with HQ and DHB. Fig.9B shows that RC provides a small and almost constant DPV response when its concentration lies at a low level. The result shows that 5-fold RC brings a less than 4.2% DPV change for the detection of HQ and DHB. Moreover, glucose, ascorbic acid and uric acid may also exist in water sample at a very low level. The investigation reveals that 10-fold above substances bring a less than 5% of the relative error. The above results indicates that proposed method is of high anti-interference ability.

3.5 Comparison study

To evaluate role of the each innovative element in the study, several kinds of materials, including GNS, HDGA-5, HDGA-6/GNS, HDGA-8/GNS, HDGA-10/GNS, HDGA-12/GMS and HDGA-20/GNS were used as the sensing materials for the electrochemical detection of HQ by the DPV method. The detection limit of different sensor basing on different material was shown in **Table 1**. For the all sensors, the overall reaction for the oxidation and reduction of hydroquinone (HQ) and benzoquinone (BQ) that carry out on the surface of the electrode is presented as following equation (3):²⁶



The mechanism is a complex combination of two one-electron transfer processes and up to two deprotonation steps, for which there are nine possible oxidation and protonation states among the reactants, intermediates, and products.²⁷ From Table 1, we can draw three conclusions. The first conclusion is that both GNS and HDGA-5 can offer an obvious electrocatalytic activity towards the reaction (3). This is because the GNS has big surface area, excellent electronic conductivity and special electrocatalytic ability.²⁸ These characteristics make the GNS can selectively catalyze the oxidization and reduction of HQ, resulting in high sensitivity of the GNS sensor. Similarly, the HDGA-5 plays very important roles in the electrocatalytic activity towards the oxidization

and reduction of HQ. On the one hand, the HDGA-5 has a high electronic conductivity, which will enhance the electron transfer between the electrode and the HQ. On the other hand, the HDGA-5 gives three-dimensional structure with a rich of open pores. The existence of open holes make the HDGA-5 can fully contact with HQ and accelerate the electrolyte transport. The two roles will bring remarkable electrocatalytic activity for the reaction (3). Second conclusion is that the HDGA-5/GNS sensor can provide a higher sensitivity than the GNS sensor and the HDGA-5 sensor, indicating that the combination of HDGA-5/GNS leads to an largely enhanced electrocatalytic activity. Because HDGA-5 In the HDGA-5/GNS hybrid acts as the connector of GNS particles to further enhance the electronic conductivity, we think that high sensitivity and fast electrochemical response of the HDGA-5/GNS sensor could be attributed to excellent electron transfer and mass transport of HDGA-5/GNS as well as remarkable synergistic effect between the HDGA-5 and the GNS. Third conclusion is that HDGA-n/GNS sensor with a higher n value can offer a higher sensitivity, indicating a better the electrocatalytic activity towards HQ. This is because a bigger n will bring a higher electronic conductivity and more stable porous structure, which greatly improve the electron transfer and electrolyte transport during the catalyzing process and results in more sensitive electrochemical response.

Table 1 Limit of detection (M) for HQ of the sensor based on the material

Material	Limit of detection	Material	limit of detection
GNS	1.84×10^{-4}	HDGA-8/GNS	8.21×10^{-11}
HDGA-5	6.22×10^{-5}	HDGA-10/GNS	5.37×10^{-11}
HDGA-5/GNS	4.30×10^{-10}	HDGA-12/GNS	3.11×10^{-12}
HDGA-6/GNS	2.17×10^{-10}	HDGA-20/GNS	6.79×10^{-13}

3.6 Application

The HDGA-5/GNS sensor was applied for the detection of HQ and DHB in several industrial water samples collected from the factory for producing HQ and DHB located in China. The concentration of HQ and DHB in water sample was determined

Table 2 Determination of HQ and DHB in water samples (N=5)

Sample	The results obtained by proposed method (μM)		The results obtained by HPLC (μM)	
	HQ	DHB	HQ	DHB
Industrial water	7.22 ± 0.14 F=1.37, t=0.13	2.16 ± 0.22 F=1.49, t=0.55	7.24 ± 0.12	2.21 ± 0.18
Well water	0.59 ± 0.06 F=2.78, t=1.28	0.42 ± 0.14 F=1.16, t=0.29	0.55 ± 0.10	0.44 ± 0.13
Surface water	0.16 ± 0.04 F=4, t=1.45	0.22 ± 0.06 F=1.77, t=1.92	0.19 ± 0.08	0.16 ± 0.08

Results expressed as: $\bar{X} \pm st\sqrt{n}$ ($n = 5$), where X is the mean of n observations of x, s is the standard deviation, t is distribution value chosen for the desired confidence level, the t- and F-values refer to comparison of the proposed method with the hexokinase method. Theoretical value at 95% confidence limits: F=6.39, t=2.78.

from the calibration curve and the value was used to calculate the concentration in the original sample. The mean \pm SD of each sample were calculated and the values are reported in **Table 2**. Table 2 shows that there is a very good agreement

between the results obtained by the proposed sensor and those obtained by high performance liquid chromatography (HPLC).

4 Conclusions

We have demonstrated a new strategy for synthesis of HDGA through multiple gel method. The as-prepared HDGA exhibits excellent mechanical and electrical properties. The study reveals that its features can be largely adjusted by controlling time of the GO gelation cycle. The HDGA/GNS as novel sensing material provides ultrasensitive electrochemical response to HQ and DHB. More importantly, the study opens an avenue for the design and synthesis of the GA materials to meet the needs of further applications in sensing, catalysis and energy storage/conversion device.

Acknowledgements

Financial support from National Natural Science Foundation of China (No.21176101), Fundamental Research Funds for the Central Universities (No.JUSRP51314B), MOE & SAFEA for the 111 Project (B13025) and country "12th Five-Year Plan" to support science and technology project (No.2012BAK08B01).

Notes and references

^a School of Chemical and Material Engineering, Jiangnan University, Wuxi, China. Fax:86051085811863; Tel:13912371144; e-mail: zaijunli@263.net

^b Key Laboratory of Food Colloids and Biotechnology, Ministry of Education, Wuxi 214122, China

Electronic Supplementary Information (ESI) available: [details of any supplementary information available should be included here]. See DOI: 10.1039/c000000x/

- H. Li, Z.B. Xia, J.Q. Chen, L. Lei and J.H. Xing, *Appl. Catal. B-Environ.*, 2015, **168**, 105.
- F. Yuan, H.M. Zhao, M. Liu and X. Quan, *Biosens. Bioelectron.*, 2015, **68**, 7.
- K.S. Novoselov, *Nature*, 2014, **505**, 291.
- H.J. Yin, H.J. Tang, D. Wang, Y. Gao and Z.Y. Tang, *ACS Nano*, 2012, **6**, 8288.
- R.Y. Li, J.J. Zhang, Z.P. Wang, Z.J. Li, J.K. Liu, Z.G. Gu and G.L. Wang, *Sensor. Actuat. B-chem.*, 2015, **208**, 421; J.J. Zhang, R.Y. Li, Z.J. Li, J.K. Liu, Z.G. Gu and G.L. Wang, *Nanoscale*, 2014, **6**, 5458; R.Y. Li, Q.F. Xia, Z.J. Li, X.L. Sun and J.K. Liu, *Biosens. Bioelectron.*, 2013, **44**, 235; Z.J. Li, X.L. Sun, Q.F. Xia, R.Y. Li, Y.J. Fang, S.P. Yang and J.K. Liu, *Electrochim. Acta*, 2012, **85**, 42; Q.F. Xia, Y.J. Huang, X. Yang and Z.J. Li, *Acta Chim. Sinica*, 2012, **70**, 1315.
- H.J. Tang, H.J. Yin, J.Y. Wang, N.L. Yang, D. Wang and Z.Y. Tang, *Angew. Chem. Int. Ed.*, 2013, **52**, 5585.
- H.J. Yin, S.L. Zhao, J.W. Wan, H.J. Tang, L. Chang, L.C. He, H.J. Zhao, Y. Gao and Z.Y. Tang, *Adv. Mater.*, 2013, **25**, 6270.
- S.L. Zhao, H.J. Yin, L. Du, G.P. Yin, Z.Y. Tang and S.Q. Liu, *J. Mater. Chem. A*, 2014, **2**, 3719.
- S.B. Ye and J.C. Feng, *ACS Appl. Mater. Interfaces*, 2014, **6**, 9671.
- L. Li, S.J. He, M.M. Liu, C.M. Zhang and W. Chen, *Anal. Chem.*, 2015, **87**, 1638; J.J. Zhang, R.Y. Li, Z.J. Li, J.K. Liu, Z.G. Gu and G.L. Wang, *Nanoscale*, 2014, **6**, 5458; R.Y. Li, J.J. Zhang, Z.P. Wang, Z.J. Li, J.K. Liu, Z.G. Gu and G.L. Wang, *Sensor Actuat B-Chem.*, 2015, **208**, 421.
- R.L. Liu, L. Wan, S.Q. Liu, L.X. Pan, D.Q. Wu and D.Y. Zhao, *Advanced Functional Materials*, 2015, **25**, 526.
- S.B. Ye, Q.L. Zhang, D.D. Hu and J.C. Feng, *J. Mater. Chem. A*, 2015, **3**, 4018.
- Q.H. Huang, F.F. Tao, L.L. Zou, T. Yuan, Z.Q. Zou, H.F. Zhang, X.G. Zhang and H. Yang, *Electrochim. Acta*, 2015, **152**, 140.
- Y.F. Dong, S.H. Liu, Z.Y. Wang, Y.B. Liu, Z.B. Zhao and J.S. Qiu, *RSC Adv.*, 2015, **5**, 8929.
- J.R. Xie, J.Y. Li, L.Q. Zhao, X.L. Zhang, B.W. Yu, R.H. Wu, R.J. Wang, J.H. Liu, F.M. Xue, and S.T. Yang, *Nanosci. Nanotech. Lett.*, 2014, **6**, 1018; J.H. Li, J.Y. Li, H. Meng, S.Y. Xie, B.W. Zhang, L.F. Li, H.J. Ma, J.Y. Zhang and M. Yu, *J. Mater. Chem. A*, 2014, **2**, 2934.
- J.F. Liang, Z. Cai, L.D. Li, L. Guo and J.X. Geng, *RSC Adv.*, 2014, **4**, 4843.
- L. Ren, K.S. Hui and K.N. Hui, *J. Mater. Chem. A*, 2013, **1**, 5689.
- L. Ren, K.S. Hui, K.N. Hui, *J. Mater. Chem. A*, 2013, **1**, 5689.
- J.H. Li, J.Y. Li, M. Hu, S.Y. Xie, B.W. Zhang, L.F. Li, H.J. Ma, J.Y. Zhang and M. Yu, *J. Mater. Chem. A*, 2014, **2**, 2934.
- F. Xiao, S.X. Yang, Z. Zhang, H.F. Liu, J.W. Xiao, L. Wan, J. Luo, S.A. Wang and Y.Q. Liu, *Scientific Reports*, 2015, **5**, 9359.
- Z.S. Wu, Y. Sun, Y.Z. Tan, S.B. Yang, X.L. Feng and K. Müllen, *J. Am. Chem. Soc.*, 2012, **134**, 19532
- S.B. Ye and J.C. Feng, *ACS Appl. Mater. Interfaces*, 2014, **6**, 9671.
- W.S. Hummers and R.E. Offeman, *J. Am. Chem. Soc.*, 1958, **80**, 1339.
- X.F. Wu, R.Y. Li, Z.J. Li, J.K. Liu, G.L. Wang and Z.G. Gu, *RSC Adv.*, 2014, **4**, 24978.
- S.Y. Zhu, W.Y. Gao, L. Zhang, J.M. Zhao and G.B. Xu, *Sensor. Actuat. B-chem.*, 2014, **198**, 388.
- N.M. Contento and P.W. Bohn, *Biomicrofluidics*, 2014, **8**, 044120
- E. Laviron and J. Electroanal, *Chem. Interfacial Electrochem.*, 1984, **164**, 213.
- Z. Zhong, J. Lin, S.P. Teh, J. Teo, F.M. Dautzenberg, *Adv. Funct. Mater.*, 2007, **17**, 1402.